JOURNAL OF COMPUTATIONAL PHYSICS 110, 234–241 (1994)

Instabilities of the Skyrme Model*

WILLIAM Y. CRUTCHFIELD AND JOHN B. BELL

Applied Mathematics Group, Lawrence Livermore National Laboratory, Livermore, California 94550

Received July 29, 1991

Previous efforts to apply finite difference methods to the Skyrme model to simulate time evolution have discovered apparent numerical instabilities. As a result, previous authors have been forced to take unusually small time-steps and introduce artificial viscosity to maintain stability. This paper analyzes finite difference schemes for the Skyrme model, demonstrates two mechanisms for the instability, and derives a corrective measure. A stable finite difference scheme in three dimensions which uses a factor of eight less memory than previous schemes is described.

1. INTRODUCTION

In 1961, Skyrme [1] presented an unusual bosonic field theory model with a non-linear time evolution equation. The model possessed solitonic solutions in addition to the usual waves of the weak field approximation. The solitonic solutions were stable because of a conserved topological charge. Skyrme identified this topological charge with the baryonic charge of elementary particle physics. The $B=1$ topological soliton was therefore identified with the nucleon. The weak field waves are found in all sectors of the model and were identified with mesons.

Recently Skyrme's model has been resurrected because of indications [2] that the quantum Skyrme model is the effective field theory of quantum chromodynamics in the limit of low energy and large N_c, where $SU(N_c)$ is the color symmetry group. Since it is widely believed that the physical value of N_c, three, is effectively close to the $N_c=\infty$ limit, this suggests that the Skyrme theory is the key to understanding low energy elementary particle physics and nuclear physics.

To this date, comparisons of the predictions of the Skyrme model with experiment have been a qualitative success. Several sectors of the model have been explored with varying degrees of completeness. In the $B=0$ sector, the low energy limit of the Lagrangian of the Skyrme model is exactly that of the extremely successful soft-pion theory [3, 4]. In the $B=1$ sector, the isolated topological soliton (Skyrmion) has been studied extensively with $O(30\%)$ agreement between its static properties and experiment [5, 6]. In the $B>1$ sector, static solutions have been found [7]. Impressively, the $B>1$ solutions reproduce qualitative aspects of the true light nuclei spectrum. For example, the most bound nucleus has $B=4$.

The Skyrme model continues to be an active area of research. However, its study is made difficult by the inaccessibility of the classical Skyrme model. No analytic Skyrme model solutions have been found. In the $B=1$ sector, the solution can be reduced to a single non-linear ordinary differential equation. But in the larger baryon number sectors, even for static solutions, no such reduction is known. Numerical solution is the only known approach.

2. BACKGROUND

In recent years, pioneering time-dependent numerical simulations [9, 10] of the Skyrme model have been performed in the $B=2$ sector of the model. These simulations are a starting point toward a semi-classical quantization of time dependent solutions of the Skyrme model in the $B=2$ sector [8]. The simulation of Verbaarschot *et al.* [10] was axially symmetric, while the Allder *et al.* calculation [9] was fully three-dimensional. Both groups used an explicit in time finite difference scheme with three time levels based on the staggered leap-frog method.

Both groups reported difficulties with numerical instabilities. Unusually small time-steps were used to enhance the stability of the simulations. The Verbaarschot *et al.* simulations typically used a CFL ratio ($\Delta t/\Delta x$) of 0.05 and introduced an artificial viscosity into their scheme to stabilize their scheme. The Allder *et al.* calculation reported using CFL ratios ranging from 0.075 to 0.013. They did not require an artificial viscosity, but they did report that even at small CFL, a calculation of the skyrmion–antiskyrmion collision process went unstable. A CFL ratio of 0.5 is more typical in finite difference schemes.

* Work performed under the auspices of the U.S. Department of Energy by the Lawrence Livermore National Laboratory under Contract W-7405-Eng-48. Partial support was provided by the Applied Mathematical Sciences Program of the Office of Energy Research under Contract W-7405-Eng-48.

0021-9991/94 $6.00

This paper details two main results which bear upon the reported numerical instabilities. First, the Skyrme model is not always a hyperbolic system of partial differential equations (PDEs). For field configurations where the local kinetic energy density is large compared to the local potential energy density, the evolution equation is of mixed type. Since the Cauchy initial-value problem is ill-posed in this case, an attempted solution will display the growth of large wave number oscillations. This is not a numerical artifact, but it is a property of the underlying PDEs. This is almost certainly the process observed by Allder *et al.* in the skyrmion–antiskyrmion collision. The simulation started in the physical, hyperbolic region and evolved in time until it entered the unphysical, non-hyperbolic region, where it became unstable. Since the Skyrme theory is derived as a low-energy approximation to quantum chromodynamics, such an artifact is not unexpected. Despite the fact that such an artifact could be expected, we have been unable to find prior discussion of this property in the literature. It is an important restriction on the use of the Skyrme model.

The second main result presented in this paper is that the leapfrog scheme presented by Allder *et al.* [9], which is apparently second order in time and space, is actually second order in space, but only first order in time. This is an artifact of their method of enforcing the chiral constraint of the model. This explains their need to use very small CFL ratios. The time-step Δt had to be small enough that the first-order temporal error would be comparable to the second-order spatial order. The time-step Δt must scale as Δx^2, so the CFL ratio would not be constant, but would decrease with Δx. We will show how to derive a modified equation analysis which demonstrates the loss of order. The analysis is generally applicable to models which enforce an algebraic constraint upon the fields at each point of space-time. We also demonstrate a new constraint which does not destroy the order of the finite difference scheme. This allows simulations to use a CFL ratio of 0.5, or an order of magnitude larger time-step than [9]. In addition, we show how to use a predictor–corrector scheme instead of the leapfrog scheme. This can result in as much as a factor of eight savings in memory use in a three-dimensional calculation.

The leapfrog finite difference scheme presented by Verbaarschot *et al.* [10] is apparently second order in Δt, although this is somewhat ambiguous. If we assume that it is second order, then there must be still a third cause of instability in the finite difference schemes. Presumably this third factor is their use of cylindrical geometry. Cylindrical coordinates introduce a restoring force in the equations of motion which is $1/r^2$ singular at the origin. We were unsuccessful in our efforts to make a stable scheme in cylindrical coordinates without artificial viscosity.

Apparently the Skyrme model has at least three different ways in which a finite difference calculation may become (apparently) unstable: non-hyperbolic regions of phase space, poor choice of constraints, and cylindrical coordinates. Previously, there was no differentiation between one cause and another, which may have given the impression that the Skyrme model was very difficult to model with finite difference methods. Hopefully, the contents of this paper will dispel the mystery surrounding this subject.

This paper contains sample numerical calculations for the Skyrme model in 3D, and an analogous model in 2D. The predictor–corrector scheme described in this paper shows second-order convergence in the sample calculations using a CFL ratio of 0.5.

3. ANALYSIS

The Lagrangian of the Skyrme model for the orthogonal group $O(N)$ is [1]

$$\mathscr{L} = -\tfrac{1}{8}(\partial_\mu \Psi_\alpha)^2 - \tfrac{1}{4}(\partial_\mu \Psi_\alpha)^2 (\partial_\nu \Psi_\beta)^2 + \tfrac{1}{4}(\partial_\mu \Psi_\alpha \partial_\mu \Psi_\beta)^2 + \tfrac{1}{2}\lambda(\Psi_\alpha^2 - 1), \tag{1}$$

where the signature of the Lorentz metric is $(-1, +1, +1, +1)$ and the parameters ε and f_π of [5] have been scaled away with coordinate transformations. The fields Ψ_α are subject to the chiral constraint

$$\sum_\alpha \Psi_\alpha^2 = 1. \tag{2}$$

The chiral constraint is enforced with the Lagrange multiplier λ.

The Lagrange equations of motion are easily derived:

$$(M_{\alpha\beta}\Psi_{\beta,t})_{,t} - (C_{\alpha\beta}\Psi_{\beta,i})_{,i} - \lambda\Psi_\alpha = 0, \tag{3}$$

where

$$M_{\alpha\beta} = \delta_{\alpha\beta}(\tfrac{1}{4} + (\partial_i \Psi_\tau)^2) - \partial_i \Psi_\alpha \partial_i \Psi_\beta \tag{4}$$

and

$$C_{\alpha\beta} = \delta_{\alpha\beta}(\tfrac{1}{4} + (\partial_\mu \Psi_\tau)^2) - \partial_\mu \Psi_\alpha \partial_\mu \Psi_\beta. \tag{5}$$

In the following, we will consider two Skyrme-type models. The $SU(2)$ Skyrme model in three spatial dimensions uses the $O(4)$ symmetry group, to which it is equivalent. We will also discuss a "pseudo-Skyrme" model in two spatial dimensions, where the symmetry group is $O(3)$. The pseudo-Skyrme model also has a topologically conserved charge, but it does not have topological solitons of finite size, as can easily be seen from scaling arguments. Numerically, the two theories are quite similar, and we will use the pseudo-Skyrme model, as well as the $O(4)$ Skyrme model in numerical tests in later sections of this paper. Being two-dimensional, the pseudo-Skyrme model is inexpensive to simulate

and makes a convenient test. For the true Skyrme model, the Lorentz index μ runs from 0 to 3, the spatial index i runs from 1 to 3, and the group indices α and β run from 1 to 4. For the pseudo-Skyrme model, the Lorentz index μ runs from 0 to 2, the spatial index i runs from 1 to 2, and the group indices α and β run from 1 to 3.

3.1. *Characteristic Analysis*

The existence of a non-hyperbolic region can be motivated with very simple physics. The equation of motion (3) has the form of a simple wave equation, in which the matrix $M_{\alpha\beta}$ plays the part of a generalized mass and the matrix $C_{\alpha\beta}$ plays the part of generalized spring constant. By its definition, the matrix M is always positive definite. The matrix C is not always positive definite. When the fields are weak, C is positive definite and diagonally dominant. Consider, however, a field configuration in which the spatial derivatives of Ψ_α are zero, but the time derivative $\partial_0 \Psi_\alpha$ is large with a norm squared (in $O(N)$ space) greater than $\frac{1}{4}$. This C matrix will have three negative eigenvalues and one positive eigenvalue. A negative spring constant causes instability. The remainder of this section substantiates this simple picture with a more careful analysis.

We will now perform a characteristic analysis to determine the speed with which small perturbations propagate in any given background field. As long as all signals propagate with real velocities, the underlying system of PDEs are hyperbolic. This is clearly the case when the background field is near the trivial vacuum solution. We will seek the occurrence of complex propagation velocities, which are the signal of non-hyperbolic behavior.

If we expand the Lagrange equation of motion (3) to a quasi-linear form we find that

$$M_{\alpha\beta}\Psi_{\beta,tt} + M_{\alpha\beta,t}\Psi_{\beta,t} = C_{\alpha\beta,i}\Psi_{\beta,i} + C_{\alpha\beta}\Psi_{\beta,ii} + \lambda\Psi_\alpha. \quad (6)$$

It is convenient for later purposes to regroup terms in the equation to separate out terms where two derivatives are applied to a field variable. This yields the expression

$$M_{\alpha\beta}\Psi_{\beta,tt} = -G_{i\alpha\beta}\Psi_{\beta,it} + J_{i\alpha\beta}\Psi_{\beta,it} - H_{ij\alpha\beta}\Psi_{\beta,ij} + C_{\alpha\beta}\Psi_{\beta,ii} + \lambda\Psi_\alpha, \quad (7)$$

where

$$G_{i\alpha\beta} = -\delta_{\alpha\beta}\Psi_{\tau,i}\Psi_{\tau,t} - \Psi_{\alpha,i}\Psi_{\beta,t} + 2\Psi_{\alpha,t}\Psi_{\beta,i} \quad (8)$$

$$J_{i\alpha\beta} = \delta_{\alpha\beta}\Psi_{\tau,t}\Psi_{\tau,i} - 2\Psi_{\alpha,i}\Psi_{\beta,t} + \Psi_{\alpha,t}\Psi_{\beta,i} \quad (9)$$

$$H_{ij\alpha\beta} = \delta_{\alpha\beta}\Psi_{\tau,j}\Psi_{\tau,i} + \Psi_{\alpha,j}\Psi_{\beta,i} - 2\Psi_{\alpha,i}\Psi_{\beta,j}. \quad (10)$$

We will now expand Ψ into the sum of a background field plus a small perturbation $\delta\Psi$. After insertion into Eq. (7), we keep only terms of lowest order in $\delta\Psi$. To ascertain whether the PDEs are hyperbolic, we must examine the high frequency limit of $\delta\Psi$. We assume that $\delta\Psi$ is varying much more quickly than the background field Ψ. In this limit, the dominant terms in Eq. (7) will be those with two derivatives acting upon $\delta\Psi$. This is a sort of eikonal approximation. The leading behavior of the small oscillations matrix at high temporal and spatial frequency is determined by the equation

$$(M\omega^2 + G_i\omega k_i - J_i\omega k_i + H_{ij}k_ik_j - Ck_ik_i)\,\delta\Psi = 0, \quad (11)$$

where the matrices M, G_i, J_i, H_{ij}, and C are constructed from the background field, Ψ_α. This is a matrix equation on the $O(N)$ group space. The points in ω, $\mathbf{k}$ space where this equation is satisfied is the dispersion curve relating ω and $\mathbf{k}$ in the high frequency limit; ω and $\mathbf{k}$ are functions of the background field, of course. The associated group vectors give the polarization associated with the given ω, $\mathbf{k}$ pair. At order $\delta\Psi$, the chiral constraint requires that $\delta\Psi$ be perpendicular to Ψ in group space. Some polarizations of the small oscillation group vector will not be perpendicular to the constraint. These polarizations are eliminated by the constraint and are not physical.

In the $O(3)$ pseudo-Skyrme model, it is possible to solve exactly for the roots of the dispersion curve (see Appendix A). For the $O(4)$ Skyrme model, it is too difficult to calculate the dispersion curve, due to the increased dimension of space and the symmetry group. Even after the constraint mode and a trivial mode have been removed, the dispersion equation is fourth order in ω. We shall concentrate instead on the more important question of when the roots of the dispersion equation become complex. By continuity, the transition between real and complex roots is marked by the formation of a double root on the real axis.

Since $\delta\Psi$ is perpendicular to Ψ, we will consider $\delta\Psi$ to be a three-dimensional vector. The matrices in Eq. (11) are constructed from three Lorentz vectors, $\partial_\mu\Psi^\alpha$, $\alpha = 1, 2, 3$. We will seek a Lorentz frame of reference in which a double root in ω is shifted to the origin, $\omega = 0$. Consider the Lorentz frame in which $\partial_z\Psi^\alpha$ is zero for $\alpha = 1, 2, 3$. It is always possible to find such a frame if at least one of the Lorentz vectors $\partial_\mu\Psi^\alpha$ is timelike. In this frame, choose $\mathbf{k}$ to lie along the z axis. In this frame and with this choice of $\mathbf{k}$, the eikonal Eq. (11) is particularly simple because the terms proportional to G_i, J_i, and H_{ij} disappear and the eikonal equation becomes

$$\det(M\omega^2 - Ck_zk_z) = 0. \quad (12)$$

If the determinant of C is zero, the above equation has a double zero at $\omega = 0$, which is the signal of the transition from real roots to complex roots. The determinant of C is a Lorentz scalar, so its vanishing is a Lorentz invariant signal of the transition from hyperbolic to mixed behavior.

In the $O(3)$ pseudo-Skyrme model, the determinant of C can be shown to be related to the Lagrangian density

$$16 \det C = 1 - 32\mathscr{L}. \tag{13}$$

This model will lose its hyperbolic nature whenever the kinetic energy exceeds the potential energy at a point by $\frac{1}{32}$ (in scaled units). The determinant of C for the $O(4)$ Skyrme model is not simply related to the Lagrangian, but the general pattern holds true that the model is completely hyperbolic when the local kinetic energy is small:

$$\begin{aligned}\det C = {} & \tfrac{1}{64} + \tfrac{1}{8}(\partial_\mu \Psi^\alpha) + \tfrac{3}{8}(\partial_\mu \Psi^\alpha)(\partial_\nu \Psi^\beta) \\ & - \tfrac{1}{8}\sum_{\mu\nu} \partial_\mu \Psi^\alpha \, \partial_\nu \Psi^\alpha \, \partial_\nu \Psi^\beta \, \partial_\mu \Psi^\beta \\ & + \tfrac{1}{3}(\partial_\mu \Psi^\alpha)^2 \, (\partial_\mu \Psi^\alpha)^2 \, (\partial_\mu \Psi^\alpha)^2 \\ & - \tfrac{1}{3}\sum_{\mu\nu\lambda} \partial_\mu \Psi^\alpha \, \partial_\nu \Psi^\alpha \, \partial_\nu \Psi^\beta \, \partial_\lambda \Psi^\beta \, \partial_\lambda \Psi^\gamma \, \partial_\mu \Psi^\gamma. \end{aligned} \tag{14}$$

For kinetic energy much larger than the potential energy, the system of PDEs will be mixed.

The physical interpretation of this non-hyperbolic behavior is that the Skyrme model has a range of validity which does not cover the whole of configuration space. The Skyrme model is derived as an effective Lagrangian in the low energy limit. High energy degrees of freedom have been integrated out in its derivation. Processes which are likely to cause a departure from the hyperbolic region are those with an intermediate state possessing quickly changing fields with relatively small spatial curvature of the fields. Annihilation of a Skyrmion and an anti-Skyrmion should be such a process since potential energy stored in the curvature of the fields will be converted to kinetic energy. Numerical simulation of a process which enters the non-hyperbolic region must be justified since the Skyrme PDEs do not represent the complete physics in this region. A process which comes close to the non-hyperbolic region is probably also inaccurately described by the Skyrme model. Numerical appoximations to the PDEs are probably unstable in a region of solution space which is slightly larger than the non-hyperbolic region of the PDEs.

This section has delineated the region of purely hyperbolic behavior for the Skyrme system of PDEs. Entry into the non-hyperbolic region is non-physical and will be signaled by unstable oscillatory solutions. The non-hyperbolic region is not a numerical artifact, but is a property of the basic partial differential equations.

3.2. *Analysis of Chiral Constraint*

The finite difference scheme of [9] is based on the Hamiltonian equations of motion

$$\partial_t \Psi_\alpha = M^{-1}_{\alpha\beta} \Pi_\beta \tag{15}$$

$$\partial_t \Pi_\alpha = \partial_i (C_{\alpha\beta} \, \partial_i \Psi_\beta) + \lambda \Psi_\alpha. \tag{16}$$

In the leapfrog scheme of [10, 9], the fields Ψ and Π are defined at alternate points of a space-time grid. Let Ψ^n and Π^n represent fields at time $t = n\,\Delta t$. Their evolution equations leap-frog one quantity over another,

$$\Psi^{n+1}_\alpha = \Psi^{n-1}_\alpha + 2\,\Delta t\, M^{-1}_{\alpha\beta} \Pi^n_\beta \tag{17}$$

$$\Pi^n_\alpha = \Pi^{n-2}_\alpha + 2\,\Delta t\, \partial_i (C_{\alpha\beta}\, \partial_i \Psi^{n-1}_\beta) + 2\,\Delta t\, \lambda^{n-1} \Psi^{n-1}_\alpha, \tag{18}$$

where the spatial derivatives are implemented as centered differences. In the absence of constraints, such schemes are second-order accurate in time and space.

The scheme of [9] enforces the chiral constraint (2) by adjusting the lagrange multiplier in (18). Consider the composition of Eqs. (17) and (18) which illustrates a full cycle of updating Ψ and Π:

$$\begin{aligned}\Psi^{n+1} = {} & \Psi^{n-1} + (2\,\Delta t)(M^{-1})^n \, \Pi^{n-2} \\ & + (2\,\Delta t)^2 \, (M^{-1})^n \, (\partial (C\, \partial \Psi^{n-1}) + \lambda^{n-1} \Psi^{n-1}). \end{aligned} \tag{19}$$

The Lagrange multiplier λ is determined by requiring the norm of the left-hand side to be one, which implies that

$$\begin{aligned} 0 = {} & 2(2\,\Delta t)\, \Psi^{n-1} (M^{-1})^n \, \Pi^{n-2} \\ & + (2\,\Delta t)^2 \, ((M^{-1})^n \, \Pi^{n-2})^2 + 2(2\,\Delta t)^2 \, \Psi^{n-1} (M^{-1})^n \\ & \times (\partial (C\, \partial \Psi^{n-1}) + \lambda^{n-1} \Psi^{n-1}) \\ & + 2(2\,\Delta t)^3 \, ((M^{-1})^n \, \Pi^{n-2})(M^{-1})^n \\ & \times (\partial (C\, \partial \Psi^{n-1}) + \lambda^{n-1} \Psi^{n-1}) \\ & + \cdots . \end{aligned} \tag{20}$$

We wish to analyze the effect of the chiral constraint upon the order of the finite difference scheme. Note that the fields composing Eq. (20) are defined at three different time levels. In order to make a comparison of the discrete equations with the PDE, we will substitute Taylor expansions for Ψ_α, Π_α, and $M_{\alpha\beta}$ about time level $n-1$ into Eq. (20). For example,

$$\Pi^{n-2} = \Pi^{n-1} - \Delta t\, \Pi^{n-1}_{,t} + \frac{\Delta t^2}{2} \Pi^{n-1}_{,tt} + \cdots . \tag{21}$$

Substitution of this and similar Taylor series into (20) yields a power series in Δt. Since all fields are evaluated at time-level $n-1$, we omit the time-level superscripts:

$$\begin{aligned} 0 = {} & 4\,\Delta t\, \Psi M^{-1} \Pi \\ & + 4\,\Delta t^2 ((M^{-1}\Pi)^2 + \Psi M^{-1} \Pi_{,t} + \Psi M^{-1}_{,t} \Pi) \\ & + 2\,\Delta t^3 (\Psi M^{-1}_{,tt} \Pi + 2 \Psi M^{-1}_{,t} \Pi_{,t} + \Psi M^{-1} \Pi_{,tt}) \\ & + 8\,\Delta t^3 (\Psi_{,t} M^{-1} \Pi_{,t} + \Psi_{,t} M^{-1}_{,t} \Pi) + \cdots . \end{aligned} \tag{22}$$

This equation should be satisfied order by order in the limit where Δt goes to zero. Consider now the tower of constraints upon the PDE which follow from taking one, two, or three time derivatives of the chiral constraint (2):

$$0 = \Psi M^{-1}\Pi \tag{23}$$

$$0 = (M^{-1}\Pi)^2 + \Psi M^{-1}_{,t}\Pi + \Psi M^{-1}\Pi_{,t} \tag{24}$$

$$0 = \Psi(M^{-1}_{,tt}\Pi + 2M^{-1}_{,t}\Pi_{,t} + M^{-1}\Pi_{,tt}) + 3(M^{-1}\Pi)(M^{-1}_{,t}\Pi + M^{-1}\Pi_{,t}). \tag{25}$$

Comparison of the identities of the PDE with the corresponding tower for the finite difference scheme (22) shows that, while the coefficients of Δt and Δt^2 in Eq. (22) are zero for solutions of the underlying PDE, the coefficient of Δt^3 is not. Note that the Lagrange multiplier enters the discrete constraint equation at $O(\Delta t^2)$. Therefore, we can compensate for the error in order Δt^3 by introducing an error in λ at order Δt. That makes the global discretization error of the constrained leap-frog method $O(\Delta t + \Delta x^2)$. This proves our assertion.

This prediction of $O(\Delta t)$ convergence was verified numerically. A series of calculations were performed on the pseudo-Skyrme model in two spatial dimensions using the leapfrog algorithm described above. The spatial grid was kept fixed: a 128^2 grid covering the region $[0, 10]^2$. The time-step was varied by factors of two over a range of 16. The initial conditions for all the experiments were the same Cauchy initial data. The $t = 0$ time level was derived trivially from the Cauchy initial data. The second time-level required by the leap-frog evolution equations was calculated to $O(\Delta t^2)$ accuracy. The initial conditions chosen correspond to a field deformed far from trivial solution and lying in the winding number one sector of the model. The initial condition was not a soliton (as remarked earlier, the pseudo-Skyrme model does not have a finite size soliton), so the field relaxes to a lower energy state by radiating waves, which are easily seen in the numerical solution. The grid is given periodic boundary conditions. For the largest time-step, 48 evolution steps were made. For the finest time-step, 768 evolution steps were made. All experiments ended at the same time, $t = 1.875$. Figures 1 and 2 show energy densities on the grid at the start and at the end of the computation. As is apparent from the figures, the initial configuration does not have complete rotational symmetry.

Table I displays the convergence test for the numerical experiments. Error is measured in the L^2 norm between adjacent experiments in the table. The L^2 error is normalized by the L^2 norm of the solution. Experiments are compared whose Δt differ by a factor of two. Results are shown for error in both Ψ and Π. Ratios of the error are also shown. If the convergence were $O(\Delta t^2)$, the ratios would be near four. The measured ratios are very close to two, indicating $O(\Delta t)$ convergence.

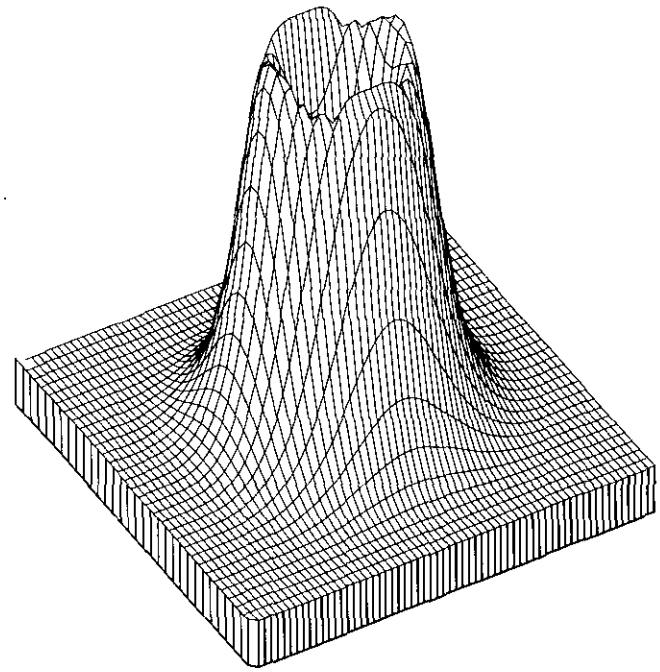

FIG. 1. Energy density as a function of position for initial field configuration used to test convergence of pseudo-Skyrme model. Energy density falls to zero at center.

There are two possible methods for fixing the loss of accuracy. The preceding analysis has identified the error in λ at $O(\Delta t)$. Therefore, a compensating term of order Δt could be added to the discrete evolution equations to compensate this error term. The remainder of this section will explore a somewhat more elegant solution.

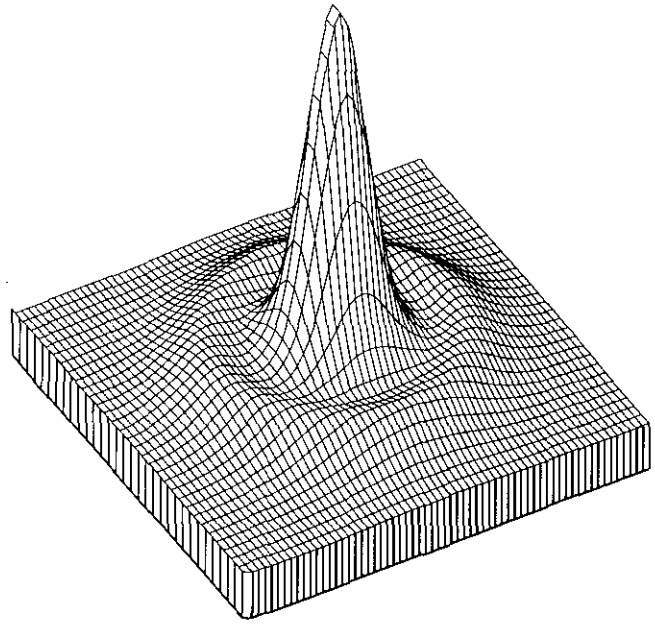

FIG. 2. Energy density as a function of position at $T = 1.875$ in convergence test of pseudo-Skyrme model. Central core has collapsed to a more compact configuration while radiating energy in the form of a mesonic wave.

TABLE I

Convergence Test for Leap-frog Method Implementing the Norm Constraint

Δt	CFL	Ψ error	Ratio Ψ error	Π error	Ratio Π error
0.0390	0.500				
		1.86e-3		0.136	
0.0195	0.250		2.07		1.97
		9.02e-4		0.0688	
0.0097	0.125		2.02		2.00
		4.466e-4		0.0344	
0.0048	0.062		2.01		2.01
		2.224e-4		0.0171	
0.0024	0.031				

Note. The grid is 128^2. Δx is held constant at 0.078 while Δt is varied. Demonstrates $O(\Delta t)$ error.

3.3. *Analysis of a New Constraint*

The constraint imposed upon the PDEs of the Skyrme model is that the norm of the field Ψ be one. It does not necessarily follow that the constraint upon the discrete evolution equation be of the same form. It is sufficient that the limit of the discrete constraint as Δx and Δt go to zero be equivalent to the chiral constraint of the PDEs. In particular, a discrete form of

$$0 = \Psi_\alpha \, \partial_t \Psi_\alpha \tag{26}$$

is an acceptable constraint. It is convenient to put this in a slightly different form. In the PDE, Ψ_α is orthogonal to all the derivatives $\partial_\mu \Psi_\alpha$. Therefore, $M^{-1}_{\alpha\beta} \Psi_\beta$ is proportional to Ψ_α. We can rewrite Eq. (26) as

$$0 = \Psi_\alpha \Pi_\alpha. \tag{27}$$

We can now repeat the previous analysis for this new constraint. The discretization of the equation of motion is exactly the same. In particular, the equation of motion contains the lagrange multiplier term. The difference is that the lagrange multiplier λ is used to enforce (27) at the new time-level, not (2). We apply the leapfrog evolution equations (17) and (18) to write $\Psi^{n+1}_\alpha \Pi^{n+1}_\alpha$ in terms of fields at earlier times. Application of the constraint yields

$$\begin{aligned} 0 = {} & (2\,\Delta t)\, \Psi^{n-1} (\partial (C^n \, \partial \Psi^n) + \lambda \Psi^n) \\ & + (2\,\Delta t)(M^{-1(n)} \Pi^n)\, \Pi^{n-1} \\ & + (2\,\Delta t)^2 \, (M^{-1(n)} \Pi^n)(\partial (C^n \, \partial \Psi^n) + \lambda \Psi^n). \end{aligned} \tag{28}$$

Note that the lagrange multiplier now appears in the expression at order Δt, rather than order Δt^2. We substitute into this equation the Taylor series expansions in Δt for Ψ^{n-1} and Π^{n-1} in terms of the fields at time-level n. The resulting expression displays the effect of the new constraints order by order:

$$0 = (2\,\Delta t)\, \Psi^n \Pi^n_{,t} + (2\,\Delta t)\, \Pi^n \Psi^n_{,t} + (\Delta t)^2 \, 0. \tag{29}$$

The $O(\Delta t)$ term is a time derivative of the new constraint, and thus zero. The $O(\Delta t^2)$ term is zero due to internal cancellations. Thus the new constraint does not have any error in order Δt, and its imposition upon a second-order finite difference scheme will not degrade the temporal error.

As before, the predicted temporal convergence was experimentally verified. The spatial domain was the same as in the previously described experiments. The initial condition was almost identical to the previous case, but the initial energy was 10% higher and the subsequent decay slightly more violent. In this test, both Δt and Δx were varied, allowing verification of both spatial and temporal error estimates. The finite difference grid varied from 32^2 in the coarsest example to 256^2 for the finest. The CFL ratio was constant in all tests as 0.5. The experiments were terminated at time 3.75, twice as long as the previous test. The results shown in Table II clearly indicate second-order convergence of the scheme.

This section has demonstrated a method for analyzing the effect of chiral constraints upon a finite difference scheme. It was shown that use of a normalization constraint in the Skyrme model (or non-linear sigma model) will degrade the natural order of convergence of the scheme. Another form of the chiral constraint was shown to preserve the natural order of convergence. Preserving the natural order of convergence is important since the effect upon the allowed Δt is quite large and grows more important as Δx is decreased. In addition to its obvious contribution to the computational cost of a simulation, the need to use abnormally small Δt suggests that the Skyrme model is numerically unstable and unsuitable for finite difference calculation, which is not true.

TABLE II

Convergence Test for Leap-frog Method Implementing the $\Psi_\alpha \Pi_\alpha = 0$ Constraint

N	Δt	Δx	Ψ error	Ratio Ψ error	Π error	Ratio Π error
32	0.156	0.312				
			5.6e-2		0.316	
64	0.078	0.156		4.24		3.75
			1.34e-2		8.43e-2	
128	0.039	0.078		4.02		3.64
			3.33e-3		2.31e-2	
256	0.019	0.039				

Note. CFL ratio is 0.5. Demonstrates $O(\Delta t^2)$ error.

4. PREDICTOR–CORRECTOR FINITE DIFFERENCE SCHEME

The finite difference schemes of [9, 10] described in the previous section are based on a staggered leap-frog scheme. In these schemes the finite difference lattice is divided into two sub-lattices, one for Ψ fields, the other for Π fields. Points of the two sub-lattices alternate with each other like the red and black squares of a checkerboard, except that the alternation takes place in four dimensions rather than two. Such a staggered scheme has disadvantages. First, it is difficult to keep track of what type of field resides at a given point. Second, some types of boundary conditions become complicated since the boundary condition will require a field value at a point where it is not defined on the grid. Lastly, it increases the memory required to describe the field configuration.

The Ψ fields can be viewed as the basic fields of the Skyrme model, and the Π fields, as auxiliary fields defined between the basic fields at half integral positions. Elimination of the Π fields would save a factor of 2^d in memory use, where d is the spatial dimension.

A finite difference scheme for the Skyrme model which does not contain the Π fields starts with the Lagrange equations of motion (3). A direct discretization of this equation is not possible because the calculation of the matrix $M_{\alpha\beta}$ at time $(n+\frac{1}{2})\,\Delta t$ requires the field Ψ at time $(n+1)\,\Delta t$, which is not yet known. This problem can be avoided by use of a predictor–corrector cycle in the scheme.

Assume that the fields Ψ_k^{n-1} and Ψ_k^n are given. Here k represents the location of a cell-centered quantity on the spatial lattice. We make a first approximation to Ψ_k^{n+1} which has an error of $O(\Delta t^2)$:

$$\Psi_k^{n+1} = 2\Psi_k^n - \Psi_k^{n-1}. \tag{30}$$

From these, we can construct spatial and temporal derivatives at times $(n-\frac{1}{2})\,\Delta t$, and approximate derivatives at $(n+\frac{1}{2})\,\Delta t$. The derivatives are logically located at cell corners; e.g., all indices are half integral,

$$(\Delta_t \Psi)_{k+1/2}^{n-1/2} = \frac{1}{2^{d-1}\,\Delta t} \sum_j (\Psi_j^n - \Psi_j^{n-1}), \tag{31}$$

where the sum extends over the cells which contain the corner. The spatial derivatives are defined similarly. The spatial derivatives at time $(n+\frac{1}{2})\,\Delta t$ have an error of $O(\Delta t^2)$, while the temporal derivatives have an error of $O(\Delta t)$. The matrices $M_{\alpha\beta}$ and $C_{\alpha\beta}$ are constructed from the derivatives at the times $(n\pm\frac{1}{2})\,\Delta t$. Interpolation is necessary since the derivatives are located at cell corners, while C and M are needed at cell faces. Substitution into the evolution equation yields a new and more accurate expression for Ψ^{n+1},

$$\Psi^{n+1} = \Psi^n + \Delta t\, M^{-1(n+1/2)} \Big((M\Psi_{,t})^{n-1/2} + \Delta t \Big(\sum \text{flux} + \cdots \Big) \Big). \tag{32}$$

The sum over fluxes is over faces of the cell. This expression has an error of $O(\Delta t^3)$. With the new value of Ψ^{n+1}, the steps above are repeated. This yields a new value for Ψ^{n+1} which has an error of $O(\Delta t^4)$. This terminates the predictor–corrector cycle since this is accurate enough for the scheme to be second-order accurate.

As before, we have verified the theoretical predictions with numerical experiments. In this case, we will present numerical experiments for the $O(4)$ Skyrme model in three dimensions, since that is the model of practical interest. A convergence study requires at least three experiments covering a factor of four refinement in Δx and Δt. We discretize a three-dimensional unit cube with 8^3, 16^3, and 32^3 points. An initial field configuration in the $B \geqslant 1$ sector of the model would be interesting, but such fields cannot be adequately represented with eight points in each linear direction. (Extensive calculations in the $B=2$ sector with a $56\times56\times28$ grid have been performed with this method [11] but they will not be reported here.) We assume that the spatial boundary conditions $\Psi_{1,2,3}$ go to zero at the boundaries; Ψ_4 goes to one at the boundaries. The initial field configuration is constructed from trigonometric functions which obey the boundary conditions

$$\begin{aligned} \Psi_1(\mathbf{x}) &= 0.8 \sin \pi x \sin \pi y \sin \pi z \\ \Psi_2(\mathbf{x}) &= 0 \\ \Psi_3(\mathbf{x}) &= 0 \\ \Psi_4(\mathbf{x}) &= \sqrt{1-\Psi_1^2}. \end{aligned} \tag{33}$$

The perturbation is strong enough that subsequent evolution is non-linear. The time derivative of the field at the initial time is taken to be identically zero. The CFL ratio for all experiments was set to 0.5. The finite difference scheme was time-stepped until $T=0.5$, which corresponds to 32 time-steps for the finest discretization. The measured convergence rate is shown in Table III. The convergence is clearly second order.

This section has shown how to replace the staggered grid of the leap-frog implementations used previously [10, 9] with a uniform finite difference grid. A predictor–corrector scheme is used to advance the Lagrange equations of motion. The new scheme uses a factor of eight less memory in three dimensions for comparable resolution. Memory consumption is an important constraint in three-dimensional calculations.

TABLE III

Convergence Test for Predictor–Corrector Scheme in 3D

N	Δx	Δt	Error	Error ratio
8	0.125	0.062		
			3.53e-3	
16	0.062	0.031		3.97
			8.88e-4	
32	0.031	0.015		

Note. CFL ratio is held constant at 0.5. The ratio indicates that convergence is second order.

5. SUMMARY

In this paper we have considered instabilities of the Skyrme model which are important in numerical simulations of the model. We have identified two instabilities and suggested the existence of a third. The first instability results from the existence of a non-hyperbolic region in the phase space of the model. Its existence is not a numerical artifact, but it is a property of the underlying partial differential equations. The second instability is an artifact of a particular method of enforcing the chiral constraint of the Skyrme model. When a more suitable discrete constraint is used, the apparent instability disappears. We have suggested that a third cause of apparent instabilities in previous work was the use of cylindrical coordinates. Cylindrical coordinates are not useful in the interesting sectors of the model, so it is no hardship to avoid their use.

Our conclusion is that instabilities are not an important factor in finite difference simulations of the Skyrme model. It is possible to simulate the Skyrme model with an order of magnitude larger timestep and a factor of eight less memory than the pioneering results of [10, 9].

APPENDIX A: DISPERSION CURVES OF THE PSEUDO-SKYRME MODEL

In this model, the dispersion relation (11) is a 3×3 matrix equation. Its characteristic polynomial has six roots. Two of the roots correspond to unphysical modes which violate the constraints. Two more roots are trivial and correspond to a wave traveling at the speed of light. The final two roots correspond to wavespeeds which depend on the background field. It is possible to solve the characteristic polynomial. Let d_μ be vectors in group space corresponding to derivatives of Ψ_α:

$$d_\mu = \partial_\mu \Psi. \tag{34}$$

We find that the roots of the characteristic polynomial are

$$\omega = \frac{-A \pm \sqrt{Z}}{D}, \tag{35}$$

where

$$A = -4k_x(d_0 \cdot d_1 + 4(d_0 \times d_2) \cdot (d_1 \times d_2)) - 4k_y(d_0 \cdot d_2 - 4(d_0 \times d_1) \cdot (d_1 \times d_2)) \tag{36}$$

$$D = 1 + 4(d_1^2 + d_2^2) + 16(d_1 \times d_2)^2 \tag{37}$$

$$Z = (k_x \quad k_y) \begin{pmatrix} z_{11} & z_{12} \\ z_{12} & z_{22} \end{pmatrix} \begin{pmatrix} k_x \\ k_y \end{pmatrix}. \tag{38}$$

The matrix $\tilde{Z}$ can be factorized as a scalar times a matrix $\tilde{Y}$,

$$\tilde{Z} = S\tilde{Y} \tag{39}$$

$$S = 1 + 4(d_1^2 + d_2^2 - d_0^2) + 16(d_1^2 d_2^2 - (d_1 \cdot d_2)^2 - d_0^2 d_1^2 + (d_0 \cdot d_1)^2 - d_0^2 d_2^2 + (d_0 \cdot d_2)^2), \tag{40}$$

where

$$\begin{aligned} y_{11} &= 1 + 4d_2^2 \\ y_{22} &= 1 + 4d_1^2 \\ y_{12} &= -4d_1 \cdot d_2. \end{aligned} \tag{41}$$

It is easily checked that the matrix $\tilde{Y}$ is positive definite, so Z can be negative only if the factor S is negative. S is proportional to the determinant of C described in the main text.

REFERENCES

1. T. H. R. Skyrme, *Nucl. Phys.* **31**, 550, 556 (1962); *Proc. R. Soc. London* **262**, 237 (1961); **260**, 127 (1961).
2. E. Witten, *Nucl. Phys. B* **160**, 57 (1979); **223**, 422 (1983).
3. B. W. Lee and H. T. Nieh, *Phys. Rev.* **166**, 1507 (1968).
4. S. Gasiorowicz and D. A. Grefen, *Rev. Mod. Phys.* **41**, 531 (1969).
5. G. S. Adkins, C. R. Nappi, and E. Witten, *Nucl. Phys. B* **228**, 552 (1983).
6. G. S. Adkins and C. R. Nappi, *Nucl. Phys. B* **233**, 109 (1984).
7. E. Braaten, S. Townsend, and L. Carson, *Phys. Lett. B* **235**, 147 (1990); also earlier work cited therein.
8. R. F. Dashen, B. Hasslacher, and A. Neveu, *Phys. Rev. D* **10**, 4114 (1974); **11**, 3424 (1975).
9. A. E. Allder, S. E. Koonin, R. Seki, and H. M. Sommermann, *Phys. Rev. Lett.* **59** (25), 2836 (1987).
10. J. J. M. Verbaarschot, T. S. Walhout, J. Wambach, and H. W. Wyld, *Nucl. Phys. A* **461**, 603 (1987).
11. W. Y. Crutchfield, N. J. Snyderman, and V. R. Brown, *Phys. Rev. Lett.* **68** (11), 1660 (1992).